2018

The combined therapeutic effects of ^{131}iodine-labeled multifunctional copper sulfide-loaded microspheres in treating breast cancer

Qiufang Liu

Yuyi Qian

Panli Li

Sihang Zhang

Zerong Wang

See next page for additional authors

Authors

Qiufang Liu, Yuyi Qian, Panli Li, Sihang Zhang, Zerong Wang, Jianjun Liu, Xiaoguang Sun, Michel Fulham, Dagan Feng, Zhigang Chen, Shaoli Song, Wei Li, and Gang Huang

Acta Pharmaceutica Sinica B 2018;8(3):371–380

Chinese Pharmaceutical Association
Institute of Materia Medica, Chinese Academy of Medical Sciences

Acta Pharmaceutica Sinica B

www.elsevier.com/locate/apsb
www.sciencedirect.com

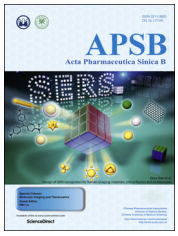

ORIGINAL ARTICLE

The combined therapeutic effects of ^{131}iodine-labeled multifunctional copper sulfide-loaded microspheres in treating breast cancer

Qiufang Liu[a,c,i,†], Yuyi Qian[b,†], Panli Li[a,c,i], Sihang Zhang[b], Zerong Wang[j], Jianjun Liu[a,i], Xiaoguang Sun[a,i], Michael Fulham[c,f,g], Dagan Feng[c,g], Zhigang Chen[h], Shaoli Song[a,c,i,*], Wei Lu[b,d,], Gang Huang[a,c,e,i,***]**

[a]*Department of Nuclear Medicine, Ren Ji Hospital, School of Medicine, Shanghai Jiao Tong University, Shanghai 200127, China*
[b]*Department of Pharmaceutics, School of Pharmacy, Key Laboratory of Smart Drug Delivery, Ministry of Education & State Key Laboratory of Molecular Engineering of Polymers, Fudan University, Shanghai 201203, China*
[c]*SJTU-USYD Joint Research Alliance for Translational Medicine, Shanghai Jiao Tong University, Shanghai 200127, China*
[d]*Department of Biomedical and Pharmaceutical Sciences, College of Pharmacy, the University of Rhode Island, Kingston, Rhode Island, RI 02881, USA*
[e]*Shanghai Key Laboratory for Molecular Imaging, Shanghai University of Medicine and Health Sciences, Shanghai 201318, China*
[f]*Department of Molecular Imaging, Royal Prince Alfred Hospital, Australia and Sydney Medical School, University of Sydney, Sydney NSW 2050, Australia*
[g]*Biomedical and Multimedia Information Technology Research Group, School of Information Technologies, University of Sydney, Sydney NSW 2006, Australia*
[h]*Centre for Future Materials, University of Southern Queensland, Springfield QLD 4300, Australia*
[i]*Institute of Clinical Nuclear Medicine, Ren Ji Hospital, School of Medicine, Shanghai Jiao Tong University, Shanghai 200127, China*
[j]*Shanghai Gezhi Middle School, Shanghai 200001, China*

Received 23 January 2018; received in revised form 28 March 2018; accepted 29 March 2018

*Corresponding authors at: Department of Nuclear Medicine, Ren Ji Hospital, School of Medicine, Shanghai Jiao Tong University, Shanghai 200127, China. Tel.: +86 21 68383850.
**Corresponding author at: Department of Pharmaceutics, School of Pharmacy, Key Laboratory of Smart Drug Delivery, Ministry of Education, and State Key Laboratory of Molecular Engineering of Polymers, Fudan University, Shanghai 201203, China. Tel.: +86 21 51980185
***Corresponding author at Department of Nuclear Medicine, Ren Ji Hospital, School of Medicine, Shanghai Jiao Tong University, Shanghai 200127, China. Tel.: +86 21 68383097
E-mail addresses: shaoli-song@163.com (Shaoli Song), wlu@fudan.edu.cn (Wei Lu), huang2802@163.com (Gang Huang).
†These authors made equal contributions to this work
Peer review under responsibility of Institute of Materia Medica, Chinese Academy of Medical Sciences and Chinese Pharmaceutical Association.

https://doi.org/10.1016/j.apsb.2018.04.001

KEY WORDS

Microspheres;
Theranostics;
Combination therapy;
Single photon emission computed tomography/computed tomography (SPECT/CT);
Photoacoustic imaging

Abstract Compared to conventional cancer treatment, combination therapy based on well-designed nanoscale platforms may offer an opportunity to eliminate tumors and reduce recurrence and metastasis. In this study, we prepared multifunctional microspheres loading ^{131}I-labeled hollow copper sulfide nanoparticles and paclitaxel (^{131}I-HCuSNPs-MS-PTX) for imaging and therapeutics of W256/B breast tumors in rats. ^{18}F-fluordeoxyglucose (^{18}F-FDG) positron emission tomography/computed tomography (PET/CT) imaging detected that the expansion of the tumor volume was delayed ($P<0.05$) following intra-tumoral (i.t.) injection with ^{131}I-HCuSNPs-MS-PTX plus near-infrared (NIR) irradiation. The immunohistochemical analysis further confirmed the anti-tumor effect. The single photon emission computed tomography (SPECT)/photoacoustic imaging mediated by ^{131}I-HCuSNPs-MS-PTX demonstrated that microspheres were mainly distributed in the tumors with a relatively low distribution in other organs. Our results revealed that ^{131}I-HCuSNPs-MS-PTX offered combined photothermal, chemo- and radio-therapies, eliminating tumors at a relatively low dose, as well as allowing SPECT/CT and photoacoustic imaging monitoring of distribution of the injected agents non-invasively. The copper sulfide-loaded microspheres, ^{131}I-HCuSNPs-MS-PTX, can serve as a versatile theranostic agent in an orthotopic breast cancer model.

1. Introduction

Breast cancer is one of the most common cancers affecting women worldwide[1,2]. In 2017, about 63,410 cases of female breast carcinoma *in situ* are predicted to be diagnosed in the United States[3]. In the clinic, surgery, radiotherapy and adjuvant chemotherapeutic agents are mostly used to eliminate the primary breast tumor while hormonal therapy and cytotoxic chemotherapy are the main systemic interventions for recurrence or distant metastasis[4,5]. However, these treatments may still result in limited therapeutic efficacy due to drug resistance or adverse effects. Even worse, insufficient treatment may accelerate the growth of tumor[6,7]. Therefore, it is imperative to develop more effective therapeutic strategies and combination therapy protocols.

With the development of nanomaterial with intense photothermal coupling effects, nanoparticle-enhanced near-infrared (NIR) laser-induced photothermal therapy (PTT) appears to be a promising strategy for cancer treatment in preclinical studies[8–10]. Additionally, these nanomaterials can provide multimodalities in cancer diagnosis and therapeutics, including drug delivery[11,12], photoacoustic imaging[13,14], and positron emission tomography/computed tomography (PET/CT) imaging[15,16]. It is attractive to design a multifunctional delivery platform that combines all these theranostic modalities in order to synergize the therapeutic efficacy, monitor the therapeutics and achieve accurate therapeutics, eventually be developed as a personalized nanomedicine.

Copper sulfide nanoparticles (CuS), with excellent optical and electrical properties have attracted increasing attention[17,18]. They serve as a promising platform for controlled drug release[11], photoacoustic imaging[19,20], PET/CT imaging[21,22] and radiotherapy[23]. Compared with most widely used photothermal agents, including metallic nanomaterials such as gold nanoparticles, CuS nanoparticles have several advantages. Firstly, CuS nanoparticles are considered biodegradable inorganic nanomaterials[11,24,25]. Secondly, the absorption wavelength of CuS nanoparticles is not affected by the solvent or the surrounding environment[26]. Thirdly, the cost of production for CuS nanoparticles is much lower.

In this study, we synthesized hollow copper sulfide nanoparticle microspheres (HCuSNPs-MS), loaded it with paclitaxel (PTX) and labeled with radioiodine-131 (^{131}I). These microspheres were applied to photothermal therapy, chemotherapy, radiotherapy, photoacoustic imaging, and single photon emission computed tomography/computed tomography (SPECT/CT) imaging in one single setting (Fig. 1). The distribution of the microspheres was imaged *via* ^{131}I-HCuSNPs-MS-PTX-mediated SPECT/CT and photoacoustic imaging. We hypothesized that ^{131}I-HCuSNPs-MS-PTX, as a combinatorial regimen, could improve the therapeutic efficacy and provide a real-time distribution of the microspheres in rats bearing an orthotopic breast cancer model.

2. Materials and methods

2.1. Synthesis and characterization of HCuSNPs-MS-PTX

HCuSNPs were prepared by the previously published method[27]. Non-radioactive iodine-labeled HCuSNPs (I-HCuSNPs) were synthesized by incubating HCuSNPs with sodium iodide (NaI) and sodium perchlorate solution ($NaClO_4$) at 32 °C for 30 min. The microspheres containing PTX and HCuSNPs were synthesized as follows: HCuSNPs (200 μL, 2.55 mg) were mixed with dichloromethane (2 mL) containing 100 mg of PLGA (Cupertino, USA, lactide:glycolide = 50:50, viscosity = 0.55–0.75 dL/g) and 5 mg of PTX (Melone Pharmaceutic, Dalian, China) with stirring at room temperature. They were then added into 2% PVA solution (Aladdin, Shanghai, China), and homogenized at 25,000 rpm for 30 s to form a w1/o/w2 multiple emulsion using magnetic stirrer. The w1/o/w2 multiple emulsion was added into 0.5% PVA solution and stirred at 1000 rpm for 3 h by magnetic stirrer. The microspheres then were purified by centrifugation at 3214 × *g* for 5 min and stored at 4 °C until use.

Transmission electron microscopy (TEM, VEGA TS5136MM, TESCAN s.r.o., Brno, Czech Republic) and scanning electron microscopy (SEM, Tecnai G2 20 TWIN, FEI company, Hillsboro,

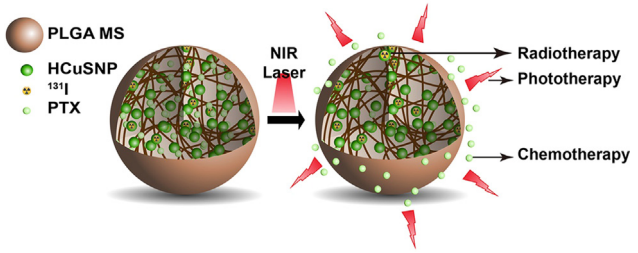

Figure 1 Scheme of ^{131}I-HCuSNPs-MS-PTX.

USA) were used to observe the morphology of HCuSNPs, I-HCuSNPs, HCuSNPs-MS, I-HCuSNPs-MS, HCuSNPs-MS-PTX and I-HCuSNPs-MS-PTX, respectively. The optical properties of the HCuSNPs and I-HCuSNPs were recorded with a UV-2401PC UV/Vis spectrophotometer (Shimadzu, Japan). Malvern Matersizer 3000 and Malvern Zetasizer Nano-90 were used to determine the size distribution of HCuSNPs, I-HCuSNPs, I-HCuSNPs-MS-PTX, HCuSNPs-MS-PTX, HCuSNPs-MS and I-HCuSNPs-MS, respectively.

2.2. *Photothermal effect of HCuSNPs-MS-PTX*

To investigate the temperature change mediated by HCuSNPs-MS *in vitro*, a 915-nm NIR laser (MDL-III-915R, CNI, Changchun, China) was used. NIR laser light (0.5 W/cm^2, 10 min) was passed through a quartz cuvette containing a HCuSNPs PBS solution (1 mg/mL, 200 μL), HCuSNPs-MS PBS solution (1 mg/mL of HCuSNPs, 200 μL) or a PBS solution (200 μL). During the laser exposure, a thermocouple was inserted into the solution to record the temperature change.

2.3. *Drug release of HCuSNPs-MS-PTX*

In the study of long-term release of PTX from HCuSNPs-MS-PTX, a solution of HCuSNPs-MS-PTX (200 μL, 0.46 mg/mL, containing 2.285 μg/mL of PTX) containing 0.5% Tween 80 was aspirated and then placed into an EP vial in a 37 °C water bath. At various times three vials were centrifuged at 13,523 × *g* for 10 min, and the free PTX was quantified by a high performance liquid chromatography (HPLC) system (LC-20AR, Shimadzu, Japan) with an SPD-M20AV photodiode array detector (Shimadzu, Japan).

The NIR-light-triggered release of PTX was investigated with two samples, which were HCuSNPs-MS-PTX precipitate (10 mg) and a PTX-MS precipitate suspended with PBS (0.01 mol/L, 200 μL, pH 7.4) containing Tween 80 (0.5%, *w/v*). The two samples were exposed to 915-nm NIR laser light at a power density of 0.5 W/cm^2 for 3 min. The above procedure was repeated three times and the solution was centrifuged at 3214 × *g* for 5 min to obtain the supernatant fraction for free PTX determination. The HCuSNPs-MS-PTX solution that did not receive laser irradiation was used as control.

2.4. *Radiolabeling of HCuSNPs-MS-PTX*

For the radiolabeling procedures, Na^{131}I (200 μL, 37 MBq) was added to HCuSNPs-MS-PTX (200 μL, 50 mg/mL, containing 0.5 mg of PTX and 0.2 mg of HCuSNPs), and then sodium perchlorate solution ($NaClO_4$) (800 μL, 0.1 mol/L) (Sigma, St Louis, MO, USA) was added with stirring. The mixture was incubated at 32 °C for 30 min. Once the reaction finished, deionized water (1 mL) was added and the sample centrifuged at 67 × *g* for 10 min to rinse free Na^{131}I. After removing the supernatants, saline (30 μL) was added to yield the final product, ^{131}I-HCuSNPs-MS-PTX. The radiolabeling yield was analyzed using thin-layer chromatography (TLC). The Whatman No. 1 filter paper was developed with deionized water.[28] A gamma counter (SN-697, Shanghai Institute of nuclear research, Rihuan Instrument Factory, Shanghai, China) was used to quantify the radioactivity. The radiolabeling yield was expressed as percentage of radioactivity of ^{131}I-HCuSNPs-MS-PTX relative to all radioiodine activity. For the study of radiolabeling stability, ^{131}I-HCuSNPs-MS-PTX was suspended in saline or 10% fetal bovine serum (FBS) and then the radiolabeling yield was measured at 30 min, 1, 2, 4, 8, 12, 24, 48 and 72 h, respectively.

2.5. *Animal preparation*

All the animal experimental procedures were in accordance with Ren Ji Institutional Animal Care. Female Sprague–Dawley rats, weight 200–250 g, were purchased from the Ren Ji Hospital Experimental Animal Center, China. Rats were housed in specific pathogen-free conditions at the laboratory animal center. To produce the orthotopic breast cancer model, W256/B cells (100 μL, 5×10^6 cells) were injected into the second mammary fat pad. When the tumor size reached 5–6 mm, the rats were ready for the experiment.

2.6. *Anti-tumor activity and histopathologic evaluation*

To evaluate the combinatorial therapeutic efficacy, rats were randomly assigned to 6 groups (A–F, $n=4$ in each group) as follows and received intra-tumoral (i.t.) injection according to the design (Fig. 2). Group A rats were injected with normal saline (control group, 30 μL). Group B rats were injected with ^{131}I-HCuSNPs-MS-PTX plus laser exposure (10 mg, 30 μL, containing 0.5 mg of PTX, 0.2 mg of HCuSNPs and 30 ± 3 MBq of ^{131}I). Group C rats were injected with ^{131}I-HCuSNPs-MS-PTX (10 mg, 30 μL, containing 0.5 mg of PTX, 0.2 mg of HCuSNPs and 30 ± 3 MBq of ^{131}I). Group D rats were injected with HCuSNPs-MS-PTX plus laser exposure (10 mg, 30 μL, containing 0.5 mg of PTX and 0.2 mg of HCuSNPs). Group E rats were injected with ^{131}I-HCuSNPs-MS plus laser exposure (10 mg, 30 μL, containing 0.2 mg of HCuSNPs and 30 ± 3 MBq of ^{131}I). Group F rats were injected with ^{131}I-HCuSNPs-MS (10 mg, 30 μL, containing 0.2 mg of HCuSNPs and 30 ± 3 MBq of ^{131}I). The groups with laser treatment were exposed to a 915-nm NIR laser at a power density of 0.5 W/cm^2 for 3 min immediately after i.t. injection. The temperature change of tumors within 4 min in each group was monitored by an infrared thermal imaging camera (DT-980, CEM, Shanghai, China) during laser irradiation.

After an ^{18}F-FDG micro PET/CT scan at 7 day-post treatment the tumors of each rats were collected and cryosectioned for hematoxylin and eosin (H&E) staining as well as Ki-67 (Novus, USA) and terminal deoxynucleotidyl transferase (TdT)-mediated dUTP nick end-labeling (TUNEL)/DAPI staining (Yeasen, China) according to the manufacturer's protocols. TUNEL-stained slides were observed under a fluorescence microscope (Zeiss Axio Observer.Z1, Germany). The major organs (liver, kidney and

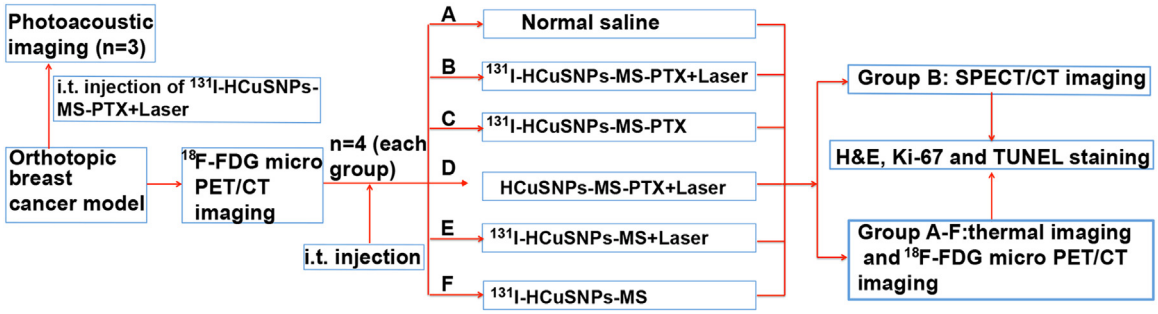

Figure 2 Scheme of the experimental design of the anti-cancer treatment in rats bearing orthotopic breast tumor. i.t. injection, intra-tumoral injection.

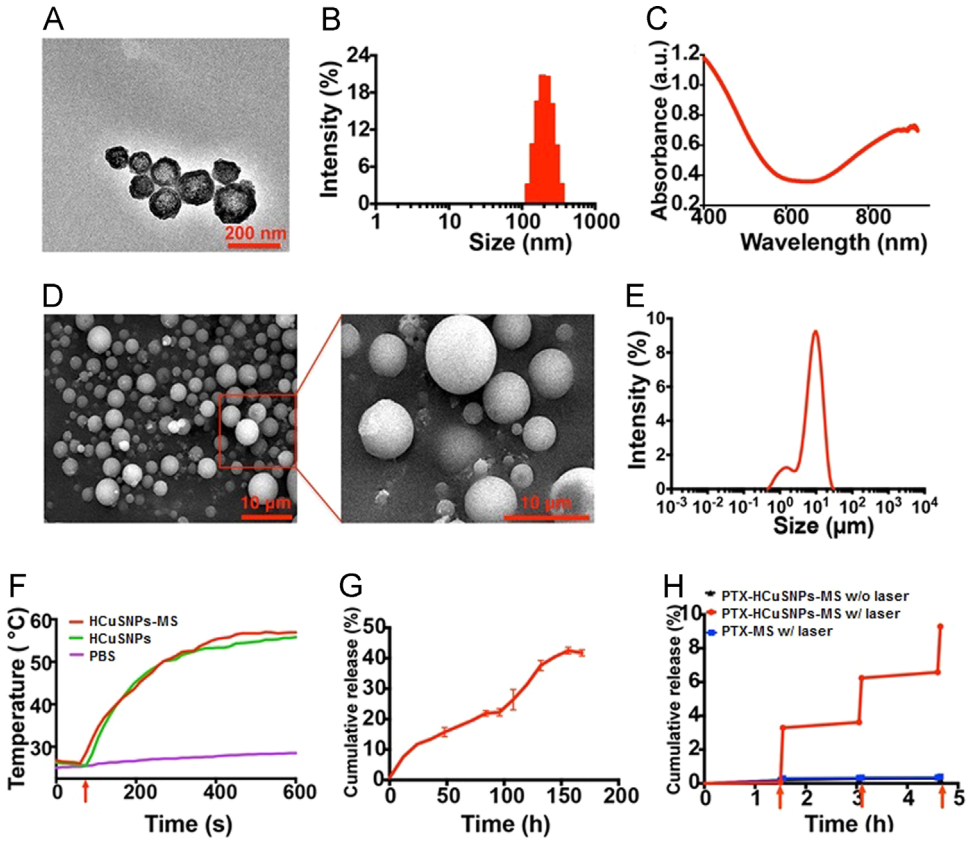

Figure 3 (A) Transmission electron microscopic image of HCuSNPs. (B) Absorption spectra of HCuSNPs. (C) Diameter distribution of HCuSNPs samples determined by dynamic light-scattering measurements. (D) Scanning electron microscopic image of HCuSNPs-MS-PTX. (E) Size distribution of HCuSNPs-MS-PTX. (F) Temperature–time profiles of HCuSNPs-MS in aqueous suspension (1 mg/mL of HCuSNPs), HCuSNPs solution (1 mg/mL of HCuSNPs), or PBS under NIR laser irradiation (915 nm, 0.5 W/cm^2). (G) Cumulative release of PTX from HCuSNPs-MS-PTX over time. (H) NIR-light-triggered release of PTX from HCuSNPs-MS-PTX (2.5 mg/mL of PTX). NIR laser light (915 nm, 0.5 W/cm^2, 3 min). Red arrows indicate laser switched on. Data are presented as Mean ± SD (n = 3).

spleen) of rats that treated with ^{131}I-HCuSNPs-MS-PTX plus laser exposure were collected for H&E staining to investigate the toxicity.

2.7. ^{18}F-FDG micro PET/CT imaging

^{18}F-FDG micro PET/CT imaging was acquired using a PET/CT scanner (Super Nova® PET/CT, PINGSENG, Shanghai, China), which has a PET spatial resolution of approximately 0.6 mm and a CT resolution of 0.2 mm, before treatment and at 1, 2, 4 and 7 day after i.t. injection. Tumor-bearing rats were anesthetized with isoflurane (2% in oxygen) and placed prone. A 30-min PET/CT scan was performed at 1 h after ^{18}F-FDG (0.3 mL, 37 MBq) i.t. injection. For data analysis, the region of interest for the tumor was drawn on CT and then copied to PET using Avatar 1.2 software (Pingseng, China). The length (a) and width (b) of the tumor, maximum standard uptake values (SUV_{max}) were determined. Tumor volume (mm^3)[29] was presented as 0.5 × a × b^2.

Table 1 Formulation of the microspheres.

Formulation	Microsphere	HCuSNPs loading (%, *w*/*w*)	EE of PTX loading (%)
A	HCuSNPs-MS-PTX	2.13±0.20	99.34±0.10
B	PTX-MS	–	98.1±0.11
C	HCuSNPs-MS	2.20±0.15	–

–Not applicable.

2.8. *SPECT/CT and photoacoustic imaging*

The tumor-bearing rats that received i.t. injection of ^{131}I-HCuSNPs-MS-PTX (10 mg, 30 μL, containing 0.5 mg of PTX, 0.2 mg of HCuSNPs and 30±3 MBq of ^{131}I) plus laser exposure underwent SPECT/CT imaging at 30 min, 24, 48 and 96 h, respectively. To minimize thyroid uptake of free ^{131}I, all rats were given water containing 0.12% of potassium iodide for 5 days before SPECT/CT imaging. SPECT/CT scans were performed on SPECT/CT system (Precedence 6, Philip, Netherlands). CT scans were performed first (using a 120 kV energy tube at 240 mA and 1 mm per scan), followed by the SPECT acquisition (128 × 128 matrix, 30 frames), which were performed by 6° angular steps in a 25 s per frame.

Another three rats bearing orthotopic breast tumors received i.t. administration of ^{131}I-HCuSNPs-MS-PTX (10 mg, 30 μL, containing 0.5 mg of PTX, 0.2 mg of HCuSNPs and 30±3 MBq of ^{131}I) underwent photoacoustic imaging. Bubble-free, clear ultrasound gel was used to facilitate acoustic contact between the transducer and the tumor. Image acquisition was conducted using a Vevo 2100 ultrasound/PA scanner with LZ400 PA probe (30 MHz linear acoustic array transducer, VisualSonics Inc., Toronto, Canada). The photoacoustic scans were conducted before and at 1, 4, and 24 h after i.t. injection, respectively. The rats were anesthetized with isoflurane during the scan. We applied several laser wavelengths, such as 750, 810, 850, 855, 895 and 915 nm for *in vivo* photoacoustic scan. A spectroscopically separated multiplexer was used to analyze the data with Vevo LAB (Ver 1.7.2) workstation software.

2.9. *Statistical analysis*

Quantitative data analysis is described as the mean±standard deviations (SD). Differences in tumor volume and SUV_{max} values on day 7 between different groups were analyzed using one-way analysis of variance (ANOVA) followed by least-significant difference (LSD) *posthoc* multiple comparison tests (SPSS 22.0, USA). A P value <0.05 was considered statistically significant. A $P<0.001$ was considered highly significant.

3. Results

3.1. *Characterization of the microsphere*

TEM images demonstrated that HCuSNPs were relatively uniform in size, with the average diameter about 191.7 nm (Fig. 3A–B).

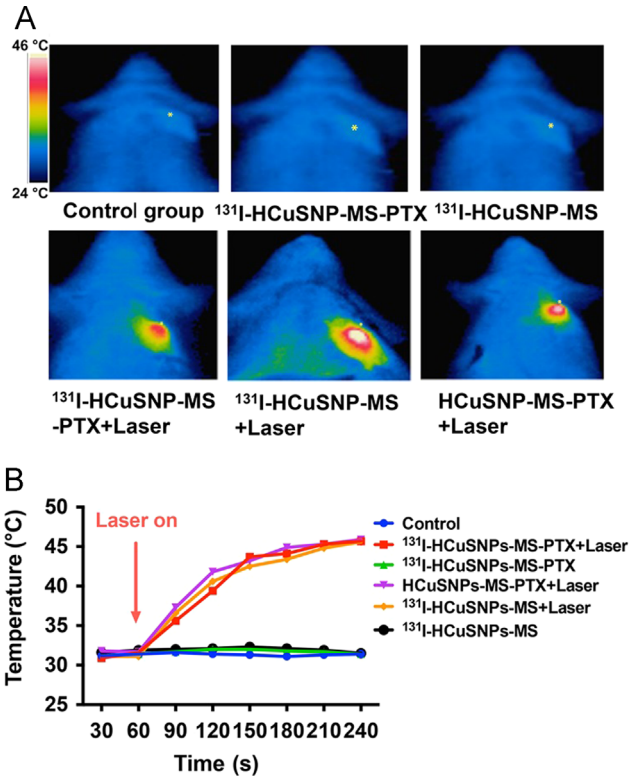

Figure 4 (A) *In vivo* thermal imaging of rats bearing orthotopic breast tumors after i.t. injection with different formulations with or without laser irradiation. (B) Temperature-time profiles of tumors following different treatments (915 nm, 0.5 W/cm^2, 3 min). Red arrows indicate laser switched on.

The HCuSNPs had a strong absorption band in the NIR region (peaked at ~900 nm, Fig. 3C). SEM images revealed the near-spherical morphology of HCuSNPs-MS-PTX, which had an average size of 9.84 μm (Fig. 3D–E). Additionally, compared with HCuSNPs, I-HCuSNPs had the similar diameter and the UV–vis spectrum of I-HCuSNPs was improved (Supplementary information Fig. S1). From the result, we found that there was no difference between I-HCuSNPs-MS-PTX, HCuSNPs-MS-PTX, HCuSNPs-MS and I-HCuSNPs-MS in size distribution (Supplementary information Fig. S1), indicating that the labeling process did not affect the characteristics of HCuSNPs-MS-PTX. PTX was loaded into PLGA microspheres with the encapsulation efficiency (EE) close to 100%. The HCuSNPs loading efficiency in the microspheres was 2.13±0.2% (Table 1). Exposed to NIR light exposure (0.5 W/cm^2) for 10 min, the temperature of HCuSNPs-MS PBS suspension (50 mg/mL of HCuSNPs-MS containing 1 mg/mL of HCuSNPs) increased from 26.4 °C to 56.1 °C (ΔT=29.7 °C, Fig. 3F). In comparison, no significant temperature change was observed in PBS following laser irradiation. There was no significant difference in temperature elevation between HCuSNPs suspensions and HCuSNPs-MS suspensions containing the same concentration of HCuSNPs (P=0.982, $P>0.05$), indicating that encapsulation of HCuSNPs into the PLGA microspheres did not affect the photothermal activity of HCuSNPs.

Fig. 3G showed that HCuSNPs-MS-PTX could provide a sustained and slow release of PTX, with a cumulative release of 7.59±0.15% at day 1 and 41.75±1.02% at day 14, respectively. This result indicated that the microspheres had the property of

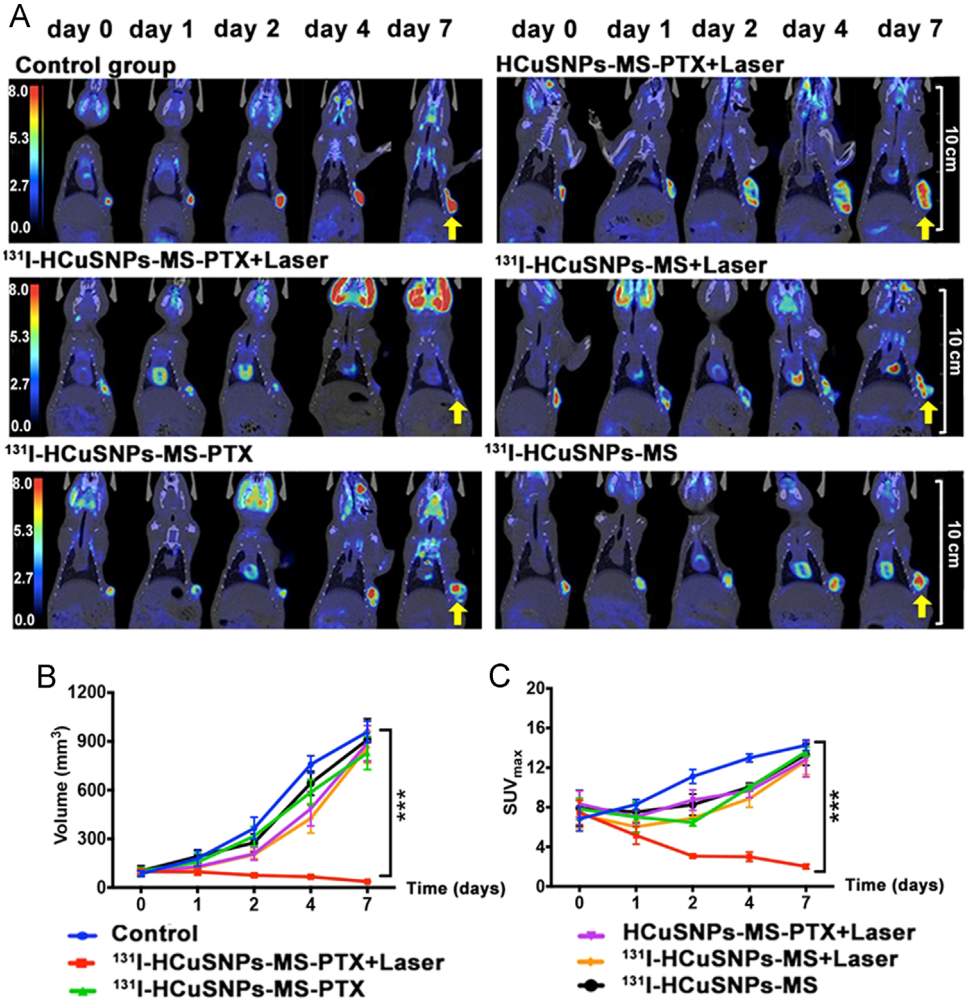

Figure 5 (A) Representative ^{18}F-FDG micro PET/CT images of rats bearing orthotopic breast tumors following different treatments. (B) Tumor volume of different groups at different time points. Arrows, tumors. (C) Tumor SUV_{max} of different treatment groups at different time-points. SUV_{max}, maximum standard uptake value. $^{***}P<0.001$, significant difference in values between the two groups on day 7. Data are presented as Mean $\pm$ SD ($n=4$).

prolonged drug release. NIR laser (0.5 W/cm^2, 3 min) at 915 nm can trigger the rapid release of PTX from HCuSNPs-MS-PTX (Fig. 3H). After the first laser exposure (0.5 W/cm^2, 3 min), the cumulative release of PTX increased from 0.6% to 3.29%. During the subsequent 1.5-h interval without laser, only 0.33% of PTX (from 3.29% to 3.62%) was released. The second and third laser irradiation cycles induced 2.62% and 2.7% of PTX release, respectively. In contrast, less than 0.4% of PTX was released over the entire experimental period without laser irradiation (Fig. 3H). The HCuSNPs-MS-PTX (containing 0.2 mg of HCuSNPs) were labeled with ^{131}I through Cu-I interaction. TLC confirmed the radiolabeling yield of ^{131}I-HCuSNPs-MS-PTX was as high as 95.8 $\pm$ 1.3%. The radiolabeling efficacy of ^{131}I-HCuSNPs-MS-PTX in saline remained at about 81.04% at 72 h and the serum stability of ^{131}I-HCuSNPs-MS-PTX decreased to 67.5% due to some deiodination.

Infrared thermography recorded the temperature changes of tumor mediated by the photothermal effects of ^{131}I-HCuSNPs-MS-PTX *in vivo*. Fig. 4 indicated that the temperature of tumors increased from 30 to 45 °C within 3 min. In comparison, there was no change of temperature detected in the tumors without laser irradiation.

3.2. *Therapeutic effect in vivo*

^{18}F-FDG micro PET/CT was used to monitor the therapeutic effect of ^{131}I-HCuSNPs-MS-PTX in an orthotopic breast cancer model. Representative micro PET/CT images showed the changes of different groups before and after the treatment (Fig. 5A). We found that the maximum standard uptake value (SUV_{max}) of ^{18}F-FDG in the control group continued to increase, while in rats treated with ^{131}I-HCuSNPs-MS-PTX plus laser treatment, ^{18}F-FDG uptakes decreased over time and reached a relatively low SUV_{max} when compared with other groups at day 7 (Fig. 5A). In other treatment groups, low ^{18}F-FDG uptake areas were mainly located in the central regions of the tumor, while the peripheral tumor tissues still exhibited high ^{18}F-FDG uptake during the treatment.

Fig. 5B shows the tumor growth curves of the six groups. Before treatment, tumor volumes were not significantly different between groups ($P>0.05$). The control group (Group A) showed a time-dependent increase in tumor volume from 95.04 $\pm$ 15.90 mm^3 (day 0) to 888.64 $\pm$ 108.66 mm^3 (day 7, $P=0.0008$, $P<0.05$). Compared with the control group, tumor growth was delayed for rats that were treated with ^{131}I-HCuSNPs-MS-PTX plus laser

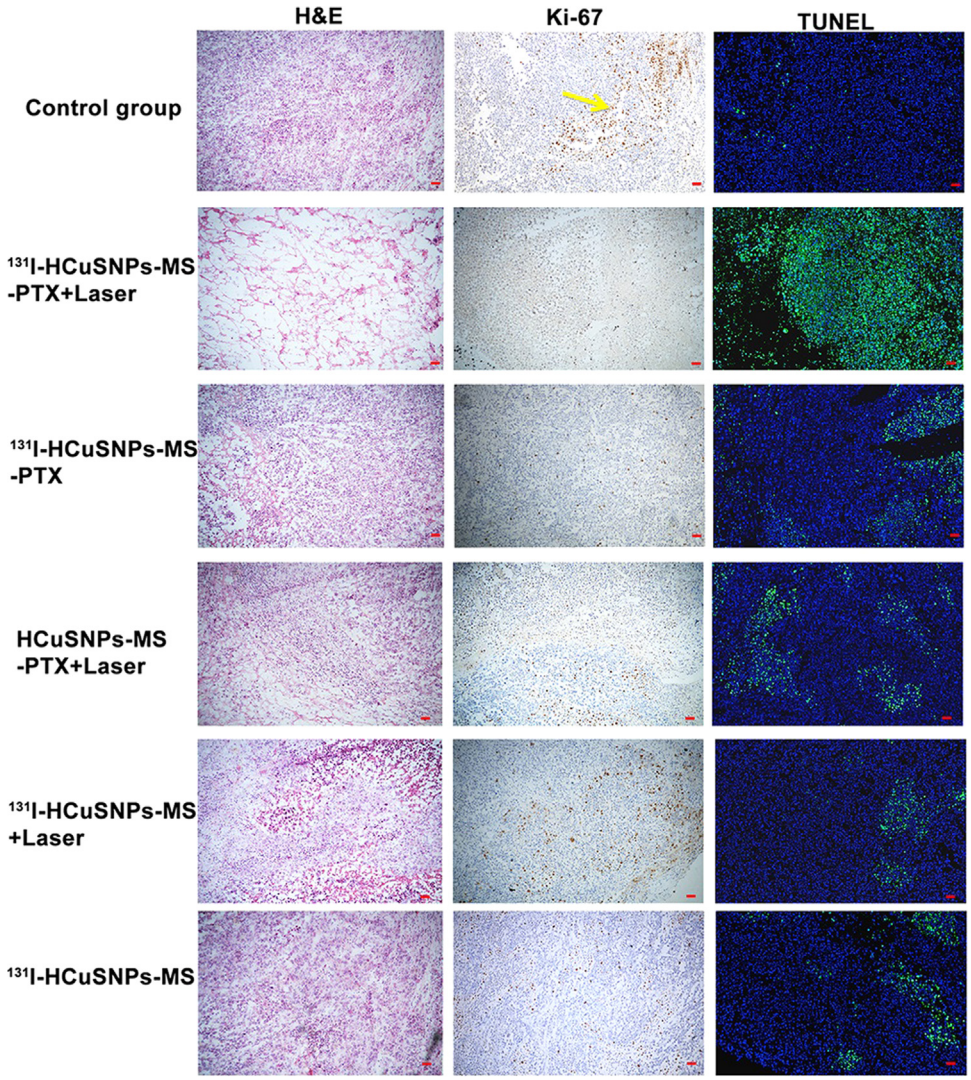

Figure 6 Rats bearing orthotopic breast tumors received i.t. injections of saline or different formulations with or without laser treatment (0.5 W/cm^2, 3 min, 915 nm). H&E staining, Ki-67 immunostaining and terminal dexynucleotidyl transferase (TdT)-mediated dUTP nick end labeling (TUNEL) staining of tumor at 7 days post-treatment. Yellow arrow, cells overexpressing of ki-67. Yellow arrow, Ki-67 positive cells. Green fluorescent, TUNEL-positive apoptotic cells; blue fluorescent, 4′,6-diamidino-2-phenylindole (DAPI)-stained nuclei. Bar, 100 μm.

exposure, and the tumor volume decreased from $98.16 \pm 14.36\,mm^3$ at day 0 to $36.92 \pm 2.3\,mm^3$ at day 7 ($P = 0.005$, $P < 0.05$). Other treatment groups showed intermediate reductions in tumor growth rates in the first several days but there was no significant difference at day 7 when compared with the untreated control group (Fig. 5B). Similar findings were observed in SUV_{max} changes (Fig. 5C). The SUV_{max} of tumors that were treated with ^{131}I-HCuSNPs-MS-PTX plus laser exposure decreased from 7.47 ± 1.24 to 2.02 ± 0.22 ($P = 0.002$, $P < 0.05$), but increased in the control group from 6.82 ± 1.22 to 14.26 ± 0.54 ($P = 0.002$, $P < 0.05$) by 7 days. In other treatment groups, SUV_{max} decreased within 1 day but increased at 7 days post-treatment.

The results of H&E staining, TUNEL and immunohistochemical staining for Ki-67 were in agreement with the ^{18}F-FDG PET/CT results, validating that ^{18}F-FDG PET/CT imaging was an accurate and non-invasive method to monitor tumor therapeutic responses. By H&E staining, tumor cells of control group (group A) displayed pleomorphism, with increases in nucleus/plasma ratios. By contrast, the tumors that were treated with ^{131}I-HCuSNPs-MS-PTX and laser exposure (group B) demonstrated remarkable degenerative and necrotic changes. The nodule mainly consisted of fibroblasts, histocytes, and lymphoplasmocytes, which surrounded a small focus of tumor cells (Fig. 6). The tumors of the control group (group A) demonstrated much higher expression of Ki-67 than tumors treated with ^{131}I-HCuSNPs-MS-PTX plus laser exposure. In other treatment groups, the necrosis mainly was located in the center of the tumor while viable tissues remained in periphery. Similarly, Ki-67 was expressed in the periphery of the tumors (Fig. 6). TUNEL staining revealed that there were more apoptotic cells in rats treated with ^{131}I-HCuSNPs-MS-PTX plus laser exposure than in other groups (Fig. 6). The H&E staining of liver, kidney and spleen did not show any obvious abnormalities, such as inflammation or lesions (Supplementary information Fig. S2).

3.3. *SPECT/CT and photoacoustic imaging*

SPECT/CT imaging revealed that ^{131}I-HCuSNPs-MS-PTX was mainly distributed to the tumors with a relatively low distribution

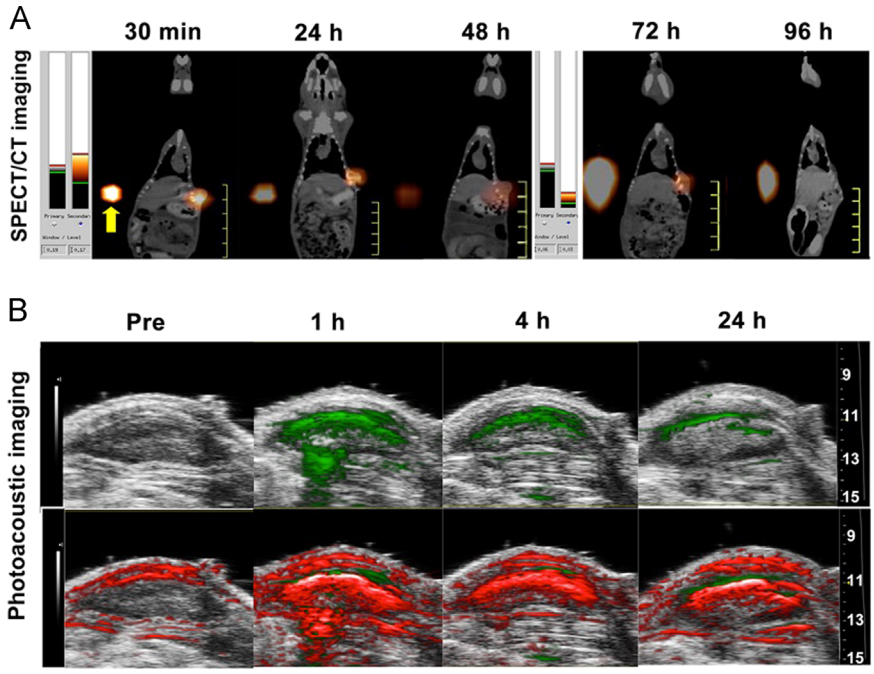

Figure 7 (A) SPECT/CT scans of rats bearing orthotopic breast tumors after i.t. injections of ^{131}I-HCuSNPs-MS-PTX (10 mg, 30 μL, containing 0.5 mg of PTX, 0.2 mg of HCuSNPs and 30 ± 3 MBq of ^{131}I). (B) Photoacoustic images of rats bearing orthotopic breast tumors before and after i.t. injections of HCuSNPs-MS-PTX (10 mg). Upper row, photoacoustic-mode imaging. Lower row, hemoglobin map of the tumor. Green, intensity of photoacoustic signals from HCuSNPs-MS-PTX. Red, intensity of photoacoustic signals from hemoglobin. Yellow arrow, standard sample (3 MBq, radiotracer solution containing 10% of the injection dose).

to other organs (Fig. 7A). The intensity of radioactivity that accumulated in tumors decreased substantially within 72 h after injection. Fig. 7B showed representative photoacoustic images of rats that were treated with ^{131}I-HCuSNPs-MS-PTX and laser exposure, before and after i.t. injection, respectively. The contour of the tumor region is clearly seen in the photoacoustic images. Most HCuSNPs-MS-PTX was located in the periphery of the tumors. The photoacoustic signal intensities in treated tumors, before and at 1, 4, and 24 h postinjection were 0.01 ± 0.05 a.u., 1.41 ± 0.12 a.u., 0.61 ± 0.02 a.u. and 0.42 ± 0.02 a.u., respectively, indicating that the signal intensity decreased over time. In addition, photoacoustic scans also demonstrated that both hemoglobin and HCuSNPs-MS-PTX were detected in the periphery of tumors (Fig. 7B). As hemoglobin is usually purely intravascular, we inferred that ^{131}I-HCuSNPs-MS-PTX was mainly distributed in perivascular tumor tissue.

4. Discussion

In this study, we successfully loaded PTX and HCuSNPs into PLGA microspheres, radiolabeled with ^{131}I and tested their efficacy in the inhibition of the growth of tumors in rats bearing an orthotopic breast cancer model. In order to investigate the combined effect of these agents, the loaded dose of PTX and ^{131}I in the ^{131}I-HCuSNPs-MS-PTX microspheres was less than the corresponding effective dose of monotherapy using either PTX or ^{131}I. The result demonstrated that the combinatorial regiment ^{131}I-HCuSNPs-MS-PTX could eliminate W256/B tumors at a relatively low dose. Combinatorial treatment has been reported to provide a more powerful strategy to eliminate tumor tissues[30,31]. Compared with the widely reported "chemo-phototherapy"[32,33], we used a radio-chemo-phototherapy strategy by labeling the nanoparticles with ^{131}I. Since the range in tissue of the ^{131}I-beta rays is approximately 2 mm[34], they can kill the peripheral tumor cells that PTX or photothermal therapy may not reach. Moreover, ^{131}I-gama rays can offer SPECT/CT imaging to detect the distribution of the microspheres.

It was noticed that the photothermal effect in our study (at most 45 °C) was mild in comparison with the temperature reported by other studies (*e.g.*, over 50 °C) for tumor cell necrosis[35,36]. Tumor temperatures above 45 °C leads to cellular injury or death due to protein denaturation[37]. The relatively mild photothermal heating (43–45 °C) induced by the shorter exposure time and the lower NIR power used here minimized normal cell death. Moreover, hyperthermia could sensitize the tumor cells to the chemotherapeutic agents[38,39].

From the ^{18}F-FDG PET/CT results we found that in groups with one or two therapeutic modals, tumoral ^{18}F-FDG uptakes decreased when compared with the control group on day 4 post-injection. However, necrotic areas may have developed in the central and relatively high-metabolizing areas remaining in the peripheral tumor tissues where the chemotherapy or photothermal therapy did not reach during the period of early treatment, which induced a recurrence on day 7. By comparison, in rats treated with ^{131}I-HCuSNPs-MS-PTX plus laser irradiation the effects of treatment were most pronounced. A complete inhibition of tumor growth was achieved as a result of the combined effects of chemotherapy, photothermal therapy, and radiotherapy. The combination of three modality treatments in a single setting reduced the dosage of each individual therapy and decreased adverse effects accordingly. Compared with multifunctional radiolabeled nanoparticles, such as CCPM-^{177}Lu[40] and ^{198}AuNP-EGCg[41], ^{131}I-HCuSNPs-MS-PTX can also serve as SPECT/CT and

photoacoustic contrast agents, allowing real-time detecting of the biodistribution and accumulation of the microspheres *in vivo* non-invasively. The SPECT/CT imaging offered high sensitivity tracking of ^{131}I-HCuSNPs-MS-PTX *in vivo*, allowing precise laser irradiation. It was demonstrated that the sustained radiation therapy was largely confined to tumors, with minimal damage to healthy surrounding tissue or other organs. Moreover, photoacoustic imaging provided useful information regarding the distribution of microspheres inside the tumor.

Due to the size of microspheres, they may not be appropriate for targeted delivery. However, our versatile molecular loading platform, with combined radio- and chemotherapeutic components, appears to be promising for local/regional therapy, such as brachytherapy and transcatheter arterial chemoembolization (TACE). Currently, localized radiotherapy with isotopes is a treatment option for many unresectable solid tumors, for example prostate cancer. However, in the clinic the implantation of millimeter size brachytherapy seeds may cause many adverse side effects or severe clinical complications, which greatly limits its applications[42,43]. Nanomedicine brachytherapy has been applied to breast cancer, prostate cancer, and glioblastoma cancer, with less severe liver, spleen or kidney toxicity[44–46]. Yook et al.[44] have reported that ^{177}Lu-labeled gold nanoparticles can serve as a novel neoadjuvant brachytherapy for locally advanced breast cancer. Compared with ^{177}Lu-labeled gold nanoparticles, our agent has several advantages. Firstly, apart from radiotherapy, ^{131}I-HCuSNPs-MS-PTX allowed a controlled drug release over a long term, which has great potential in improving therapeutic efficacy. Secondly, HCuSNPs-MS-PTX can be labeled with iodine-125 (^{125}I) as the method of labeling with ^{131}I. The radiolabeling process is straightforward and the radioisotope ^{131}I and ^{125}I are widely used in clinic and are easier to produce than ^{177}Lu[47,48]. Therefore, our multifunctional agent is a promising candidate to eliminate unresectable solid tumor tissues due to the synergistic effect. Additionally, because the size of ^{131}I-HCuSNPs-MS-PTX is controllable, we can also synthesis the microspheres with an appropriate size for transcatheter arterial chemoembolization to treat hepatocellular carcinoma.

5. Conclusion

Our study confirmed that hollow copper sulfide-loaded microspheres, ^{131}I-HCuSNPs-MS-PTX, could serve as a versatile theranostic agent in an orthotopic rat breast cancer model. The combination of photothermal, chemo- and radio-therapies in a single setting can help to eradicate the tumor completely and reduce the effective dose of monotherapy and decrease side effects accordingly. Simultaneously, SPECT/CT and photoacoustic imaging mediated by ^{131}I-HCuSNPs-MS-PTX can intuitively monitor the distribution of the injected agents *in vivo*.

Acknowledgments

This work was partially supported by National Natural Science Foundation of China (Nos. 81771861, 81471708, 81673018, 81530053, 81471685), the award of the “National Youth Thousand Talents Plan” of China, the Program for Professor of Special Appointment (Eastern Scholar) at Shanghai Institutions of Higher Learning (No. 2012-05), Shanghai Municipal Education Commission—Gaofeng Clinical Medicine Grant Support (No. 20172010), 2018 Shanghai Scientific and Technological Innovation Program (No. 18410711200) and the Ph.D. Innovation Fund of Shanghai Jiao Tong University, School of Medicine (BXJ201821).

Appendix A. Supporting information

Supplementary data associated with this article can be found in the online version at doi:10.1016/j.apsb.2018.04.001.

References

1. Ferlay J, Steliarova-Foucher E, Lortet-Tieulent J, Rosso S, Coebergh JW, Comber H, et al. Cancer incidence and mortality patterns in Europe: estimates for 40 countries in 2012. *Eur J Cancer* 2013;**49**:1374–403.
2. Chowdhury P, Nagesh PK, Khan S, Hafeez BB, Chauhan SC, Jaggi M, et al. Development of polyvinylpyrrolidone/paclitaxel self-assemblies for breast cancer. *Acta Pharm Sin B* 2017. Available from: http://dx.doi.org/10.1016/j.apsb.2017.10.004.
3. Siegel RL, Miller KD, Jemal A. Cancer statistics. *CA Cancer J Clin* 2017;**67**:7–30.
4. Harris SR, Schmitz KH, Campbell KL, McNeely ML. Clinical practice guidelines for breast cancer rehabilitation: syntheses of guideline recommendations and qualitative appraisals. *Cancer* 2012;**118**:2312–24.
5. Tryfonidis K, Senkus E, Cardoso MJ, Cardoso F. Management of locally advanced breast cancer-perspectives and future directions. *Nat Rev Clin Oncol* 2015;**12**:147–62.
6. Chabner BA, Roberts Jr. TG. Timeline: chemotherapy and the war on cancer. *Nat Rev Cancer* 2005;**5**:65–72.
7. Ceelen W, Pattyn P, Mareel M. Surgery, wound healing, and metastasis: recent insights and clinical implications. *Crit Rev Oncol Hematol* 2014;**89**:16–26.
8. Zhou M, Song S, Zhao J, Tian M, Li C. Theranostic CuS nanoparticles targeting folate receptors for PET image-guided photothermal therapy. *J Mater Chem B* 2015;**3**:8939–48.
9. Her S, Jaffray DA, Allen C. Gold nanoparticles for applications in cancer radiotherapy: mechanisms and recent advancements. *Adv Drug Deliv Rev* 2017;**109**:84–101.
10. Shanmugam V, Selvakumar S, Yeh CS. Near-infrared light-responsive nanomaterials in cancer therapeutics. *Chem Soc Rev* 2014;**43**:6254–87.
11. Ramadan S, Guo L, Li Y, Yan B, Lu W. Hollow copper sulfide nanoparticle-mediated transdermal drug delivery. *Small* 2012;**8**:3143–50.
12. Shalgunov V, Zaytseva-Zotova D, Zinchenko A, Levada T, Shilov Y, Andreyev D, et al. Comprehensive study of the drug delivery properties of poly(L-lactide)-poly(ethylene glycol) nanoparticles in rats and tumor-bearing mice. *J Control Release* 2017;**261**:31–42.
13. Li Y, Liu G, Ma J, Lin J, Lin H, Su G, et al. Chemotherapeutic drug-photothermal agent co-self-assembling nanoparticles for near-infrared fluorescence and photoacoustic dual-modal imaging-guided chemo-photothermal synergistic therapy. *J Control Release* 2017;**258**:95–107.
14. Song J, Yang X, Yang Z, Lin L, Liu Y, Zhou Z, et al. Rational design of branched nanoporous gold nanoshells with enhanced physico-optical properties for optical imaging and cancer therapy. *ACS Nano* 2017;**11**:6102–13.
15. Goel S, England CG, Chen F, Cai W. Positron emission tomography and nanotechnology: a dynamic duo for cancer theranostics. *Adv Drug Deliv Rev* 2017;**113**:157–76.
16. Liu Q, Zhou M, Li P, Ku G, Huang G, Li C, et al. 64 CuS-labeled nanoparticles: a new sentinel-lymph-node-mapping agent for PET-CT and photoacoustic tomography. *Contrast Media Mol Imaging* 2016;**11**:475–81.
17. Pissuwan D, Nose K, Kurihara R, Kaneko K, Tahara Y, Kamiya N, et al. A solid-in-oil dispersion of gold nanorods can enhance

transdermal protein delivery and skin vaccination. *Small* 2011;**7**:215–20.
18. Li Y, Lu W, Huang Q, Huang M, Li C, Chen W. Copper sulfide nanoparticles for photothermal ablation of tumor cells. *Nanomedicine (London)* 2010;**5**:1161–71.
19. Ku G, Zhou M, Song S, Huang Q, Hazle J, Li C. Copper sulfide nanoparticles as a new class of photoacoustic contrast agent for deep tissue imaging at 1064 nm. *ACS Nano* 2012;**6**:7489–96.
20. Zhou M, Ku G, Pageon L, Li C. Theranostic probe for simultaneous *in vivo* photoacoustic imaging and confined photothermolysis by pulsed laser at 1064 nm in 4T1 breast cancer model. *Nanoscale* 2014;**6**:15228–35.
21. Liu Q, Zhou M, Li P, Ku G, Huang G, Li C, et al. ^{64}CuS-labeled nanoparticles: a new sentinel-lymph-node-mapping agent for PET-CT and photoacoustic tomography. *Contrast Media Mol Imaging* 2016;**11**:475–81.
22. Zhou M, Melancon M, Stafford RJ, Li J, Nick AM, Tian M, et al. Precision nanomedicine using dual positron emission tomography and magnetic resonance temperature imaging-guided photothermal therapy. *J Nucl Med* 2016;**57**:1778–83.
23. Zhou M, Zhao J, Tian M, Song S, Zhang R, Gupta S, et al. Radio-photothermal therapy mediated by a single compartment nanoplatform depletes tumor initiating cells and reduces lung metastasis in the orthotopic 4T1 breast tumor model. *Nanoscale* 2015;**7**:19438–47.
24. Guo L, Yan DD, Yang D, Li Y, Wang X, Zalewski O, et al. Combinatorial photothermal and immuno cancer therapy using chitosan-coated hollow copper sulfide nanoparticles. *ACS Nano* 2014;**8**:5670–81.
25. Guo L, Panderi I, Yan DD, Szulak K, Li Y, Chen YT, et al. A comparative study of hollow copper sulfide nanoparticles and hollow gold nanospheres on degradability and toxicity. *ACS Nano* 2013;**7**:8780–93.
26. Goel S, Chen F, Cai W. Synthesis and biomedical applications of copper sulfide nanoparticles: from sensors to theranostics. *Small* 2014;**10**:631–45.
27. Zhou M, Zhang R, Huang M, Lu W, Song S, Melancon MP, et al. A chelator-free multifunctional [^{64}Cu]CuS nanoparticle platform for simultaneous micro-PET/CT imaging and photothermal ablation therapy. *J Am Chem Soc* 2010;**132**:15351–8.
28. Ji Y, Zhan Y, Jiang C, Jiang X, Gao M, Liu W, et al. Improvement of solubility and targetability of radioiodinated hypericin by using sodium cholate based solvent in rat models of necrosis. *J Drug Target* 2014;**22**:304–12.
29. Naito S, von Eschenbach AC, Giavazzi R, Fidler IJ. Growth and metastasis of tumor cells isolated from a human renal cell carcinoma implanted into different organs of nude mice. *Cancer Res* 1986;**46**:4109–15.
30. He C, Duan X, Guo N, Chan C, Poon C, Weichselbaum RR, et al. Core-shell nanoscale coordination polymers combine chemotherapy and photodynamic therapy to potentiate checkpoint blockade cancer immunotherapy. *Nat Commun* 2016;**7**:12499.
31. He C, Liu D, Lin W. Self-assembled core-shell nanoparticles for combined chemotherapy and photodynamic therapy of resistant head and neck cancers. *ACS Nano* 2015;**9**:991–1003.
32. Deng X, Liang Y, Peng X, Su T, Luo S, Cao J, et al. A facile strategy to generate polymeric nanoparticles for synergistic chemo-photodynamic therapy. *Chem Commun (Camb)* 2015;**51**:4271–4.
33. Jiang D, Gao X, Kang T, Feng X, Yao J, Yang M, et al. Actively targeting D-alpha-tocopheryl polyethylene glycol 1000 succinate-poly (lactic acid) nanoparticles as vesicles for chemo-photodynamic combination therapy of doxorubicin-resistant breast cancer. *Nanoscale* 2016;**8**:3100–18.
34. Champion C, Zanotti-Fregonara P, Hindie E. CELLDOSE: a Monte Carlo code to assess electron dose distribution—S values for ^{131}I in spheres of various sizes. *J Nucl Med* 2008;**49**:151–7.
35. Hu D, Zhang J, Gao G, Sheng Z, Cui H, Cai L. Indocyanine green-loaded polydopamine-reduced graphene oxide nanocomposites with amplifying photoacoustic and photothermal effects for cancer theranostics. *Theranostics* 2016;**6**:1043–52.
36. Greenhalgh TA, Dearman C, Sharma RA. Combination of novel agents with radiotherapy to treat rectal cancer. *Clin Oncol (R Coll Radiol)* 2016;**28**:116–39.
37. He X, Wolkers WF, Crowe JH, Swanlund DJ, Bischof JC. *In situ* thermal denaturation of proteins in dunning AT-1 prostate cancer cells: implication for hyperthermic cell injury. *Ann Biomed Eng* 2004;**32**:1384–98.
38. Li Y, Deng Y, Tian X, Ke H, Guo M, Zhu A, et al. Multipronged design of light-triggered nanoparticles to overcome cisplatin resistance for efficient ablation of resistant tumor. *ACS Nano* 2015;**9**:9626–37.
39. Pai CL, Chen YC, Hsu CY, Su HL, Lai PS. Carbon nanotube-mediated photothermal disruption of endosomes/lysosomes reverses doxorubicin resistance in MCF-7/ADR cells. *J Biomed Nanotechnol* 2016;**12**:619–29.
40. You J, Zhao J, Wen X, Wu C, Huang Q, Guan F, et al. Chemoradiation therapy using cyclopamine-loaded liquid–lipid nanoparticles and lutetium-177-labeled core-crosslinked polymeric micelles. *J Control Release* 2015;**202**:40–8.
41. Shukla R, Chanda N, Zambre A, Upendran A, Katti K, Kulkarni RR, et al. Laminin receptor specific therapeutic gold nanoparticles (^{198}AuNP-EGCg) show efficacy in treating prostate cancer. *Proc Natl Acad Sci U S A* 2012;**109**:12426–31.
42. Yoshioka Y. Current status and perspectives of brachytherapy for prostate cancer. *Int J Clin Oncol* 2009;**14**:31–6.
43. Patel RR, Arthur DW. The emergence of advanced brachytherapy techniques for common malignancies. *Hematol Oncol Clin North Am* 2006;**20**:97–118.
44. Yook S, Cai Z, Lu Y, Winnik MA, Pignol JP, Reilly RM. Intratumorally injected ^{177}Lu-labeled gold nanoparticles: gold nanoseed brachytherapy with application for neoadjuvant treatment of locally advanced breast cancer. *J Nucl Med* 2016;**57**:936–42.
45. Moeendarbari S, Tekade R, Mulgaonkar A, Christensen P, Ramezani S, Hassan G, et al. Theranostic nanoseeds for efficacious internal radiation therapy of unresectable solid tumors. *Sci Rep* 2016;**6**:20614.
46. Shultz MD, Wilson JD, Fuller CE, Zhang J, Dorn HC, Fatouros PP. Metallofullerene-based nanoplatform for brain tumor brachytherapy and longitudinal imaging in a murine orthotopic xenograft model. *Radiology* 2011;**261**:136–43.
47. Lin CY, Lin CL, Huang WS, Kao CH. Risk of breast cancer in patients with thyroid cancer receiving or not receiving ^{131}I treatment: a nationwide population-based Cohort study. *J Nucl Med* 2016;**57**:685–90.
48. Avram AM, Esfandiari NH, Wong KK. Preablation ^{131}I scans with SPECT/CT contribute to thyroid cancer risk stratification and ^{131}I therapy planning. *J Clin Endocrinol Metab* 2015;**100**:1895–902.